Decoding the Speed and Motion Direction of Moving Targets using a Turtle Retinal Patch Model

Mervyn P. B. Ekanayake, Bijoy K. Ghosh, *Fellow, IEEE,* and Philip Ulinski

***Abstract*—Using a model patch of the turtle retina, we show that it is possible to decode the motion direction and speed of a point target moving in the visual space of a turtle, using the spatiotemporal response of a retinal patch. Turtle retina primarily contains two kinds of cells that are functionally different – the intensity sensitive A cells and the motion direction sensitive B cells. The cells are clustered primarily in the vicinity of a visual streak and in this paper we analyze the decodability of a circular patch located near the center of the streak. The patch is subjected to a moving point target, as input, that passes through its center along various different angles and speed. The first problem considered is to detect the motion direction of a point target assuming that its speed is known. In the second problem, we assume that both the speed and the motion directions are unknown. The problem considered is to estimate the speed and use this information to detect the motion direction. The two problems are handled using, primarily, the following two methods – one using principal component analysis of the neural signals viewed as a spatio-temporal response of the patch and the other using a suitable pooling process where a selected set of neural responses, over a 'subpatch,' are pooled. Counting rate of the pooled process is used for the purpose of decoding. An important conclusion of this paper is to show that –** *The B Cells outperform the A Cells* **in detecting target motion direction particularly when the target speed is a priori unknown.**

***Index Terms*—visual streak, retinal patch, principal components, pooled point processes, direction sensitive cells.**

I. Introduction

THIS paper continues our ongoing study of modeling the visual pathway of freshwater turtles. Earlier we had already shown (see [1], [2], [3], [4], [5]) that visual inputs produce waves that propagate across the visual cortex of freshwater turtles and visual information is encoded in the cortical waves. In all of our prior models, the visual input was directly incident on the lateral geniculate, completely bypassing the retina. The purpose of this paper is to add a model of the retinal cell to the pathway and to study how retinal signals encode a moving point target incident on a small **retinal patch**. The target is moving with a constant, possibly unknown, velocity along directions that are spread across the entire 360°.

Turtle Retinal ganglion cells have an excitatory center and inhibitory surrounding ("ON" type), inhibitory center and excitatory surrounding ("OFF" type) or the "ON-OFF" type which has an excitatory center, an inhibitory annulus followed by an outermost excitatory surrounding (e.g. see [6]). Some of the turtle retinal cells are sensitive to the direction of the optical flow of an image sequence, (e.g. [7], [8]). These cells are called, "direction sensitive cells" or the 'B Cells.' The other cells, which are not sensitive to the direction of motion (but are sensitive to the intensity of the target), are called the 'A cells.' The 'A Cells' can be ON or OFF type, where as, the 'B Cells' are ON-OFF type. The 'A cells' have a larger cell body (soma size) as well as a larger dendritic arborization, resulting in a larger receptor field, compared to the 'B cells' (see [6]). On the other hand, the 'A cells' are smaller in number compared to the 'B cells' on the turtle retina [9], [10].

Turtle retina effectively encodes the motion parameters of moving targets in its visual space (see [11]). The retinal ganglion cells encode input signals using a sequence of spikes. We reproduce the spike generation process, using a set of filters, which model layers of rods and cones in the retina. The filters for the 'B cells' have been shown in Fig. 1. The 'A cells' have a similar block diagram for which the directional filters are absent. The output of the filters are incident on a single compartment spike generating neuronal cell, with primarily Sodium and Potassium channels, modeled using Hodgkin-Huxley equations (see [12]). For a physiologically detailed model of a single cell, that includes many additional channels, we would refer to the Ph.D. thesis of Ekanayake [13]. Also we remark that retina has been modeled in other animals as well, for example salamander [14] and cat [15].

We consider a patch of the retina (shown in Fig. 2a) and circular targets that are moving with unknown constant speed and motion direction. Our objective is described in the following two problems. In the first problem we consider targets that are moving along an unknown direction with fixed speed that are assumed to be known a priori. Our goal is to detect the motion direction of the unknown target. In the second problem we assume that both the direction and the speed of the targets are unknown. Our objective is to first estimate the speed and use this information to detect the motion direction.

Two methods to detect the unknown motion direction of the target is now described. In the first method, we use **Principal Component Analysis** (see [1], [16]). The spike sequence generated by the model patch is low pass filtered, separately for each cell in the patch, producing a vector of continuous signals, which approximates the spike rate of the cells in the patch. The vector of spike rate functions, over a suitable time window, are projected as points on a cartesian coordinate

This material is based upon work supported in part by the National Science Foundation under the grant number BIC 0523983 and ECCS 1029178. Any opinions, findings, and conclusions or recommendations expressed in this material are those of the author(s) and do not necessarily reflect the views of the National Science Foundation.

M. P. B. Ekanayake and B. K. Ghosh are with the Department of Mathematics and Statistics, Texas Tech University, Lubbock, TX 79409, USA. e-mail: mpb.ekanayake@ttu.edu.

P. S. Ulinski was with the Department of Organismal Biology and Anatomy, University of Chicago, Chicago, IL 60637 USA. He is now deceased.

system using Principal Component Analysis (pca). We model these points as realizations of a Gaussian process, conditioned on the direction of motion and detect the 'target motion direction' using the well known Maximum Likelihood Estimation Method ([17]). In the second method, we hypothesize that the pattern of spiking activity in a cell, can be described by a class of Point Process, called 'Self Exciting Poisson Process' (see [18]). We use the fact that a collection of such processes can be **pooled** together, and under an appropriate hypothesis (see [18]), the pooled processes can be modeled as an inhomogeneous Poisson Process. We pool together the spiking activities of a subpatch of cells in a patch and represent the pooled activities as an inhomogeneous vector Poisson process. We estimate intensity functions for each component of this process, conditioned on the input direction of the target. The direction of motion of an unknown input can be detected using estimates of the intensity function vector.

The second method can also be used to estimate the speed and detect the motion direction of a target. This is done by first constructing a vector of subpatches (see Fig. 4b) within a chosen patch. Estimates of intensity functions of the spike activities (pooled over subpatches) are subsequently computed. Next, we calculate the width of the intensity function (see Fig. 5a for half height pulse width) and use this parameter to estimate the target speed. In order to estimate target motion direction, we rescale the intensity function to a standard unit length, i.e. to the $[0, 1]$ interval, where time is measured in seconds. The amplitudes of the intensity functions are also normalized to a unit height. For a suitably chosen set of subpatches, the rescaled intensity functions are intensity functions of an inhomogeneous Poisson Process. The motion directions are detected using *maximum likelihood estimates* (see (11) for the log likelihood function). We remark that in order to model the intensity function from an inhomogeneous Poisson Process, the required subpatches are not what has been shown in Fig. 4b, but are smaller in size.

The motion directions can also be detected from the rescaled intensity functions by representing these functions as points on a principle component space and modeled as a Gaussian Process. The details are similar to the first method except that the detection algorithm is repeated over each and every subpatches described in Fig. 4b. The final decision of the detection algorithm is made by a majority vote [19], [20], one vote for every subpatch.

II. Model of Retinal Cells

Turtles, being vertebrates, have a multi layered retinal structure. From the point of view of visual signal processing, it has layers of photoreceptive cells, consisting of cones and rods. These cells are synaptic to a layer of ganglion cells which give rise to the optic nerve fibers (see [11]).

We model the layer of photoreceptive cells as a cascade of filters which represent key functions, including the spatial and temporal variation of sensitivity of the receptor field (see [21]) and direction sensitivity only for the 'B cells' (see [8]). Fig. 1 shows the block diagram of the filter cascades of the 'B cells' ('A cells' have a similar block diagram but are not directionally sensitive). The ganglion cells are modeled as firing neurons using the Hodgkin-Huxley (HH) model using parameters from [22], [23]. Noise is modeled as an input to the HH model. In the following subsections the function of the major components of the filter model are described. This model was originally reported by Baker [24] and we would like to refer to [13] for details.

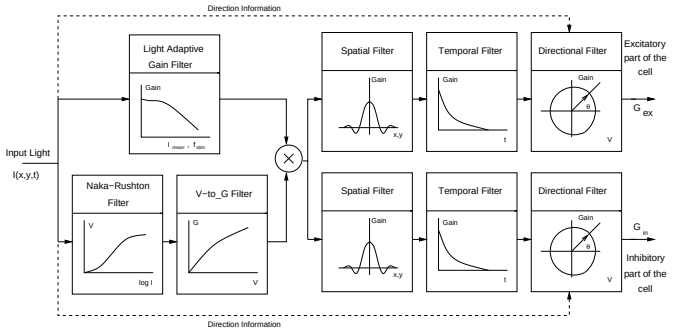

Fig. 1: Block diagram of the filters present in 'B Cells'. The first set of 3 filters are saturating filters. The next set of filters are spatial, temporal and directional filters of a 'B cell' model. They are separated into an excitatory and an inhibitory part. The 'A cells' (not shown in the figure) do not have the directional filters.

1) Basic Conductance Signal: The basic conductance signal is computed at each spatial location. It is generated in two steps. First, the visual (light) signal is passed through a nonlinear saturation filter, called the Naka-Rushton Filter [25].

$$V_R = V_{RM} \frac{I^n}{I^n + a^n}, \tag{1}$$

where, I_n is the input light intensity at each spatial location, V_{RM}, a and n are constants for a cell.

Subsequently, the resulting V_R signal is passed through another filter G to obtain the basic conductance signal [25]. The filter G is described as

$$G(V_R) = g_{max} + \frac{E_{rest} - V_R - E'_{rest}}{R_{in}\left(E_{rest} - V_R - E_{Na^+}\right)} \tag{2}$$

where, V_R is the voltage signal created at the previous block, E_{rest}, E'_{rest}, E_{Na^+}, are respectively the resting membrane potential, resting membrane potential with all Na channels closed, and the sodium channel reversal potential, and g_{max} is a constant. The conductance signal generated in this step is subsequently modulated using various filters, viz. spatial, temporal and directional filters.

2) Spatial Filters: The spatial filters characterize the inherent receptor field structure of the ganglion cells [26]. In terms of implementation, this filter multiplies the conductance signal at each spatial location. The 'A cells' could be one of two kinds. The first kind, termed as A-ON cells, have excitatory center and an inhibitory surrounding. The second type of cell, called A-off cell, has an inhibitory center and excitatory surrounding. The receptor field structure of 'A cells' are modeled as being the difference of Gaussian functions

$$G_A(x, y) = k_e e^{-r^2/2\sigma_e^2} - k_i e^{-r^2/2\sigma_i^2}, \tag{3}$$

where $r = \sqrt{x^2 + y^2}$ with (x, y) being the spatial coordinates. The 'B cells' have a slightly more complicated structure.

They have an excitatory center, an inhibitory rim and another excitatory rim after that. This structure is modeled as a Gabor function:

$$G_B(x, y) = ke^{-r^2/2\sigma^2} \cos(2\pi fr). \quad (4)$$

3) Directional Filters: The 'B cells' are sensitive to the direction of the motion θ of the visual stimuli [26] and are modeled with the directional filter

$$d(\theta) = a\left(1 + b\cos(\theta - \phi)\right), \quad (5)$$

which multiplies the basic conductance signal at each spatial location. This directional filter is only applied to the 'B cells'. The parameter values a and b are different for the excitatory and the inhibitory parts. The angle parameter ϕ is the preferred direction of the cell [8], and 3 principle preferred directions are assumed to be $180°$, $40°$ and $-75°$.

4) The Light Adaptive Filter: The input light is used to compute the gain of the light adaptive gain filter. This is basically a low pass filter calculated at each spatial location and is given by

$$H(f, I_0) = H_n\left(\frac{A(f)}{1 + I_0 B(f)}\right). \quad (6)$$

The computed gain multiplies the conductance signal. The filter transfer function is dependent on the mean light intensity, I_0, and it is expressed as a function of frequency of light variation, f, (not the frequency of the light as in the electromagnetic spectrum). The filter has a large gain for low frequencies and low light intensities. Effectively, it enhances slow varying dim signals, which could otherwise go unrecognized [27].

5) Temporal Filter: The temporal filter models how past inputs control the future outputs of the retinal ganglion cells [28]. It is essentially a low pass filter. Since the temporal responses of the excitatory and inhibitory areas are not the same, two different temporal time constants have been assumed. It follows that the temporal response is modeled using transfer function

$$s(t) = ae^{-t/\tau_a} - be^{-t/\tau_b}, \quad (7)$$

where a, b, τ_a and τ_b are constants.

6) Neuron Model: The output of the filter cascade is fed to the Hodgkin-Huxley model stage as a synaptic current I_{in}, using the equation $I_{in} = G_{ex}(V - E_{ex}) + G_{in}(V - E_{in})$, where V is the post synaptic membrane potential of the cell, $E_{ex} = 0$ mV is the excitatory synaptic potential and $E_{in} = -70$ mV is the inhibitory synaptic potential.

The retinal Ganglion Cell is modeled as a single compartmental model with ionic channels for sodium, potassium and calcium. Further more, channels representing the dynamics of the calcium concentration and after hyperpolarization potassium conductance are also employed. As such, the neural model implements a detailed Hodgkin-Huxley equation, accounting for all the essential channels including the calcium channel adaptation.

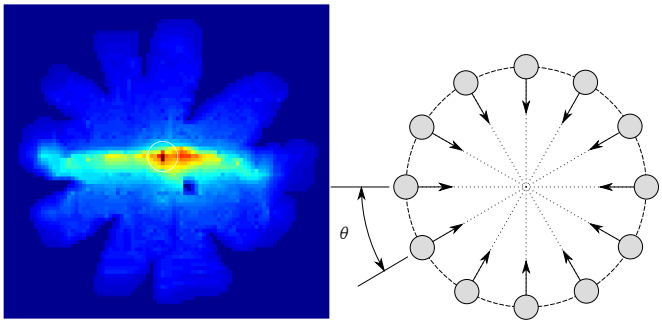

(a) Cells on the turtle retina (b) Paths of the incident light spot

Fig. 2: (Left) Distribution of all cells on the retina showing the visual streak. The circle on the center of the streak indicates the location of the retinal patch analyzed in this paper. (Right) The input to the retina is a circular spot of light (drawn to scale with respect to the size of the patch of 3 mm diameter) moving from one end of the patch to the other in a straight line, passing through the center.

7) Noise Model: Under the natural set up, the spiking pattern is not completely deterministic. There are various uncertainties which cause the membrane potential to jitter and even produce "arbitrary" spikes or "miss" producing spikes (for example, see [29]). Therefore, a realistic model should have some stochastic component. In neurons, most of these "random" behavior occurs due to random fluctuations in the channel conductances. Therefore, we introduce the stochasticity via a Gaussian random current with zero mean and variance calibrated in such a way that we would, on average get two or three random spikes every ten milliseconds when no input is present.

8) Model Implementation: We have used MATLAB ([30]) to implement the filter cascade and GENESIS neural simulator ([31]) to implement the Hodgkin-Huxley model. The Gaussian random noise is added as an input current to the HH model. The response of the model neuron has been calibrated by comparing the results to the recordings reported in the literature (e.g. [6]).

III. Construction of a Retinal Patch

The ganglion cells on a turtle retina are distributed in such a way that the it is possible to observe a high density of cells along a line, called the **visual streak**. The spatial distribution of turtle ganglion cells on the retina has been studied in [9]. It reports the cell density over a multitude of vertical and horizontal transects as to cover the entire retina. We interpolate the data provided, using a two dimensional cubic spline to compute the cell density (both A and B types combined) over the whole retina.

A subsequent paper, [10] reports the distribution of size of ganglion cells on some selected sites over the retina of turtles. By inspecting the data reported in [10], we can identify that histogram of the size of the cell body is bimodal. We fit this data on the size distribution of cells at the reported sites, with the sum of two Gaussian distributions. As reported in [6], the 'A cells' are larger in soma size compared to 'B cells.' Therefore, we claim that the 'A cells' are distributed with the higher mean cell size and the 'B cells' are distributed with the smaller cell size. The percentage of 'A cells' calculated at each

site was then interpolated over the entire retina again using a two dimensional cubic spline. Multiplying the percentage of 'A cells' with the cell density data calculated as above, we obtain the distribution of 'A cells' over the entire retina. This procedure is now repeated for the 'B cells.' Fig. 2a shows the distribution of the entire population of retinal ganglion cells.

Since the turtle retina has 350–390 thousand cells, we use about 1% of that for constructing large-scale models of the full retina. Majority of the cells are B cells. The 'B cells' are divided in to 3 equal groups, corresponding to 3 distinct direction preferences. The 'A cells' are divided in to two equal groups based on their receptor field structure, known as the A-ON and the A-OFF. The three groups of the 'B cells' and the two groups of 'A cells' are randomly sprinkled over the retina to match the computed density functions.

A circular retinal patch has been used to obtain results reported in this paper. The patch is taken to be the cells which are contained in a three millimeter circular disc centered at the location with maximum cell density on the visual streak. It has a total of 520 cells, of which 54 are A-ON cells, 55 are A-OFF cells. The 'B cell' counts are 134, 136 and 141 for the three angle preferences of 180°, 40° and -75° respectively. These are the mean of the groups of directional sensitive cells reported in [8].

IV. Description of two different simulations using the retinal patch

In this section we detail two different, yet related, simulations on the model retinal patch. In the first simulation, we collect data to detect unknown motion direction of a point target assuming that the speed of the target is known. In the second simulation, we collect data to estimate the speed and use this information to detect motion direction of a point target, assuming that both of these parameters are unknown. In both simulations, the input is a spot of light on a dark background. The patch is circular of diameter 3 mm and the size of the spot is one tenth the size of the patch.

A. Simulation I: Detection of Motion Direction

We consider a circular retinal patch (shown in Fig. 2a) and assume that a point target moves with a constant velocity through the center of the patch. The target takes 0.8 seconds to cross the patch. The simulation pool consists of motion directions between 0° (i.e. the target moves from left to right) and 358° at steps of 2°. It follows that we have 180 different directions of motion, each motion direction is simulated 60 times. Objective of this simulation is to study how different cell types discriminate directions of motion.

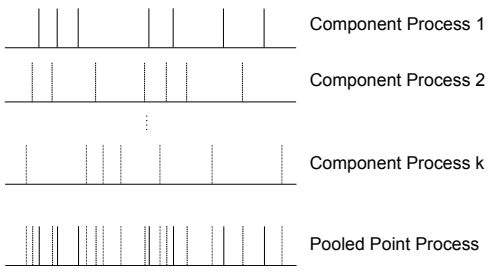

Fig. 3: An example of pooling spike events, demonstrated using k randomly chosen cells.

B. Simulation II: Estimation of Speed and Motion Direction

In this simulation, we use twelve different angles from 0° to 330° at steps of 30°. We have the target move along each direction at 9 different speeds. As the speed varies, the target takes between 0.4 seconds to 2 seconds to diametrically cross the patch. In all, we have 108 different speed/angle combinations (i.e. 108 different velocities). Each combination is simulated 60 times. In addition to these evenly spaced simulation points, we also generate intermediate test points with five intermediate speeds and sixty intermediate angles. These intermediate points are each simulated 10 times.

V. Algorithms

The two main tools for analysis we use are the theory of self exciting point processes [18], [32] and the principal component analysis (pca) [16]. In the first simulation described in IV-A, the activities of the cells in the patch are low pass filtered individually. The smoothed activity functions are represented using pca by considering the entire patch as the spatial window and over a suitable time window (see Fig. 4a). The spatiotemporal activity of the retinal patch is thus represented as a strand conditioned on the target direction. Maximum likelihood detection is performed assuming that the strand is a Gaussian random process, the details are similar to what was done by Du et. al. [3]. Alternatively, the spike activities of the cells are pooled over a subpatch, and the intensity function of the pooled process, a Poisson Process, is computed. This step is repeated over a vector of subpatches. The obtained vector of intensity functions is now used to detect the target motion direction.

In the second simulation described in IV-B, the speed of the target is estimated from the intensity function of the pooled spike activities. The pooling process is similar to what was

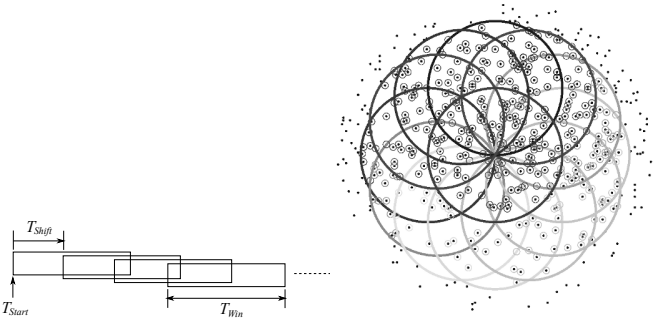

(a) Sliding time windows (b) A set of subpatches

Fig. 4: (Left) Sliding time windows used in this paper. The window size is T_{Win} milliseconds and the window shifts T_{Shift} milliseconds at a time starting from T_{Start}. (Right) A set of subpatches used for pooling to estimate the speed of the unknown target in Simulation II. Different shades of circles indicate different subpatches. The same subpatches have also been used to detect target motion direction using pca and voting methods.

described for the first simulation except that in this case the subpatches considered are comparatively bigger in diameter (see Fig. 4b). The estimation is carried out from the 'half height pulse widths' of the associated intensity functions. Using the estimated speeds, the target directions are inferred using two different methods. In the first method, the spike pattern of each cell is rescaled to be distributed over an unit length in seconds. The rescaled spike activities are pooled over a vector of smaller subpatches, as in the first simulation, and the corresponding intensity functions are modeled as a Poisson Process. The target motion directions are detected using Maximum Likelihood Estimation. In the second method, the intensity functions are first computed over a vector of bigger subpatches (of Fig. 4b) and are subsequently rescaled using the estimated target speeds to be distributed over an unit length in seconds. The target motion directions are detected from the re-scaled intensity functions using pca, over each and every subpatch. The pca is carried out over a moving time window and we assume that the principal component (pc) points form a Gaussian Process. Over every subpatch, target detection is carried out by running a maximum likelihood detection algorithm for Gaussian Processes (see Van Trees [17]). The final target direction is inferred using a majority vote over the subpatches (see [19], [20]).

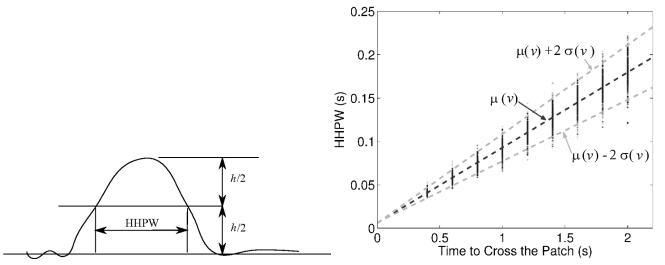

(a) Pulse showing half height pulse width (b) Mean and standard devition of the HHPW

Fig. 5: (Left) Half height pulse width has been illustrated. (Right) Variation of half height pulse width (HHPW) plotted with respect to time the target takes to cross the patch in seconds. For a specific speed, the HHPW varies for different angles of target movement and noise. The variation of mean $\mu(v)$ and standard deviation $\sigma(v)$ are displayed on the graph.

A. Principal Component Analysis

Since the model patch consists of spatially distributed cells, each producing a temporal response of spike patterns, the resulting observation data (i.e. the spike sequences) has a large dimension. Principal component analysis (pca), also known as the discrete Karhunen Loeve transform (KLT) (see [16]) can be effectively used to represent a high dimensional data as points in a lower dimensional space. We apply the pca technique twice, once along the spatial and the next along the temporal dimensions using a sliding detection time window (see Fig. 4a). A two step pca analysis has already been carried out in ([1], [3]) for the purpose of detecting locations and velocities of point targets using a model of the turtle cortex. In this paper, we analyze the retinal patch response using moving 20 ms time windows. The retinal responses are projected onto a 6 dimensional principal component space at the end of the two step pca.

It may be inferred from the principal component analysis, that at a specific time, the 'Principal Component Points' are spread around a mean location dependent on the direction angle of the target. By inspection, Gaussian distribution seems to be a reasonable hypothesis for this data. This hypothesis can be verified statistically by a normality test. In our analysis, the resulting data points are tested for normality using Lilliefors Test (see [33]). We consider null hypothesis that the sample in each dimension of PC points comes from a normal distribution, against the alternative that it does not come from a normal distribution. The test fails to reject the null hypothesis at 5% significance level. This test is an adaptation of the well known Kolmogorov-Smirnov (KS) test ([34]) and does not require the specification of the parameters of a target normal distribution. Failing to reject the null hypothesis, would imply that the sample data points can be assumed to be distributed 'as a normal distribution.'

The principal component points are viewed as a Gaussian Process over time, conditioned on the motion directions of the target. Using a standard detection process, (see Van Trees [17], Du [3]) the target directions are detected.

B. Analysis using Point Process Models

Many studies [35], have explored the possibility of applying the theory of counting processes towards analyzing neural signals. The general hypothesis of 'evolution without aftereffects,' of homogeneous or inhomogeneous Poisson processes, does not apply for neural data because there is a brief refractory period after a spike discharge. With this assumption relaxed, we can hypothesize that the spike sequences recorded from a cell are realizations of *self-exciting point processes*. A limit theorem for mutually independent pooled point processes, possibly self-exciting point processes, states that the pooled process converge in distribution to an inhomogeneous Poisson process (see [18] for details). Fig. 3 illustrates the process of pooling. To statistically verify that a certain candidate sequence of spikes, is a Poisson Process, one can apply the Spike Rescaling Theorem ([18], [36]).

It may be noted that an inhomogeneous Poisson process is governed by an intensity function $\lambda(t)$. The probability of having n spikes between the starting time 0 and arbitrary positive time t is given by

$$\Pr[N_{0,t} = n] = \frac{(\Lambda(t))^n}{n!} \exp\left(-\Lambda(t)\right), \tag{8}$$

where $\Lambda(t) = \int_{\tau=0}^{t} \lambda(\tau)\, \mathrm{d}\tau$.

The first challenge of analyzing the response of a retinal patch, under this framework, is to estimate the intensity function $\lambda(t)$, which customarily is estimated using binning methods (see [36], [35], [37]). However, we propose to estimate $\Lambda(t)$ directly where

$$\Lambda(t) = \lim_{K\to\infty} \frac{1}{K} \sum_{k=1}^{K} N_{0,t}^{(k)} \tag{9}$$

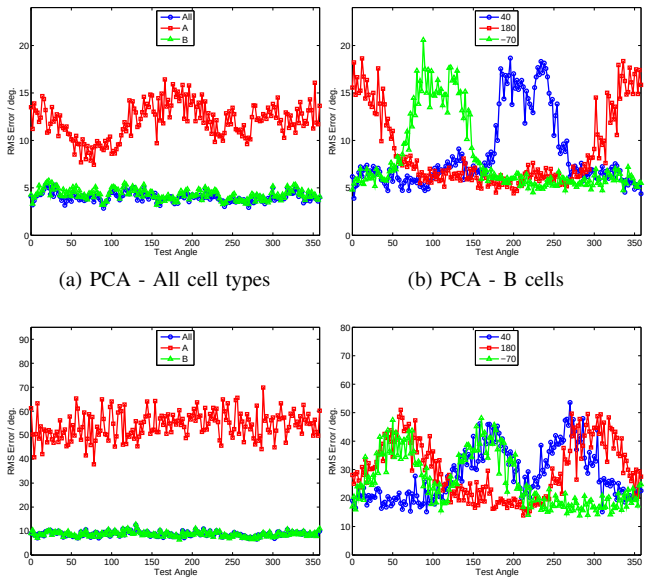

(a) PCA - All cell types (b) PCA - B cells

(c) PPM - All cell types (d) PPM - B cells

Fig. 6: Root Mean Square Error of detection using principal component analysis (PCA) and poisson process model (PPM) for Simulation I. The detection error is calculated using a 20 ms time window starting at 400 ms. At the speed used, the target takes 800 ms to traverse the retinal patch.

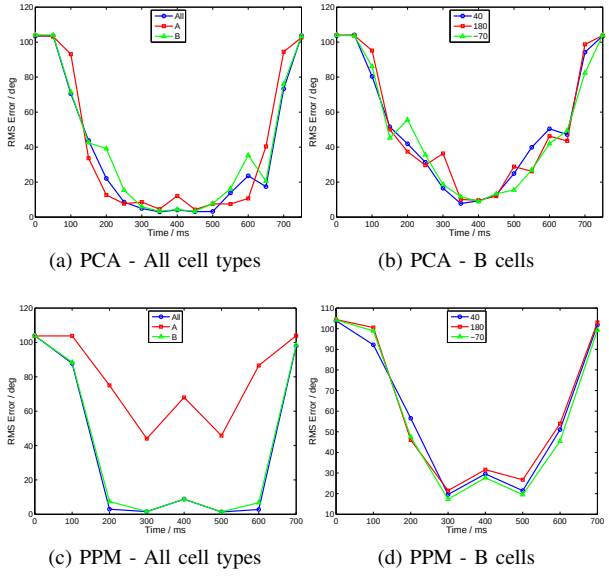

(a) PCA - All cell types (b) PCA - B cells

(c) PPM - All cell types (d) PPM - B cells

Fig. 7: Variation of root mean square error of detection using principal component analysis (PCA) and poisson process model (PPM), with time has been plotted for Simulation I. The detection error is calculated using a 20 ms time window starting at the indicated time points.

and where $N_{0,t}^{(k)}$ is the total number of spikes occurred during the time interval $(0, t]$. We call $\Lambda(t)$, the cumulative spike count between 0 and t. In practice, we would calculate the mean of $N_{0,t}^{(k)}$ over the test simulations and smooth $\Lambda(t)$ using a smoothing spline [38], [39] or a low pass filter.

VI. Analysis

Two problems that we consider in this paper have already been described in section IV. In 'problem one,' our goal is to detect the motion direction of a target assuming that its speed is constant. The data has been collected using Simulation I, wherein the motion direction is varied in steps of 2° from 0° to 358° (see Fig. 2b). The response of the patch is recorded and analyzed using the principal component analysis (pca) method as well as using the point process models (ppm), obtained by pooling a small number of adjacent cells. In 'problem two,' our goal is to detect the motion direction of a target in spite of the fact that its speed is unknown but assumed to be a constant. The data has been collected using Simulation II, wherein the motion direction is varied in steps of 30° from 0° to 330° (see Fig. 2b), and the speed of the target is assumed to vary. As a first step, speed of the target is estimated using the width of the half height pulse obtained by pooling cells in a subpatch shown in Fig. 4b. The pulse is the intensity function of the process obtained by pooling the cells in a subpatch, shown in Fig. 4b. In order to detect the motion direction, the estimated target speed is used to rescale activities of the cells, as already summarized in section V.

A. Detection of Motion Direction

In this subsection, our goal is to analyze the data obtained in Simulation I, wherein the assumption is that the target moves with a constant and known velocity.

1) Principle Component Analysis: In the principal component approach, a patch response is calculated by combining the spiking activities of each and every cells in the patch. For each cell, the spike activity pattern is low pass filtered and one obtains a continuous signal that measures the instantaneous spike counting rate. The filtered activity patterns are aggregated over the entire patch using a two step pca, once over space covering the patch and next over a time window of width 20 ms. The starting time point of the time window is shifted at 50 ms (see Fig. 4a).

A two step pca over a specific window gives a vector in $\mathbb{R}^n$, where n is taken to be 6 in this paper. The principal component vector calculated using a particular time window can be uniquely identified and indexed by the starting time of the window. It would follow that, we can view the principal component vector as an n dimensional stochastic process $\boldsymbol{P}(t)$, where t is the starting time of the window.

At a particular time t_*, the principal component vector $\boldsymbol{P}(t_*)$ can be modeled as realizations of a multivariate ($n = 6$) Gaussian distribution with mean $\boldsymbol{\mu}$ and covariance matrix Σ. Using multiple simulations it is possible to estimate the mean vector $\boldsymbol{\mu}_\theta$ and covariance matrix Σ_θ for each angle θ. We use 50 simulations for each angle to obtain these parameters. Once the parameters are obtained, we use a different set of 10 simulations for each angle to test the algorithm. The likelihood function of the motion direction is given

$$L(\theta|\boldsymbol{r}) = \frac{\exp\left(-(\boldsymbol{r}-\boldsymbol{\mu}_\theta)^\top \Sigma_\theta (\boldsymbol{r}-\boldsymbol{\mu}_\theta)/2\right)}{\sqrt{2^k \pi^k \left|\Sigma_\theta\right|}}, \qquad (10)$$

where $\boldsymbol{r}$ is one sample of $\boldsymbol{P}(t_*)$. The objective is to find θ that would maximize $L(\theta|\boldsymbol{r})$. We claim that the corresponding θ is the maximum likelihood estimate given $\boldsymbol{r}$ (see [17], [40]).

We apply this technique of maximum likelihood estimates for different time points and for different cell types and the results are summarized in VII

2) Method using Point Process Models: The first step in using point process models is to pool together the activities of cells within a subpatch. The process of pooling together the spike activities over a subpatch has been illustrated in Fig. 3. The patch size needs to be carefully chosen in order to control the number of cells that are to be pooled together. The spiking activity of a single retinal ganglion cell has an internal memory and a refractory period, and as a result the spike times do not satisfy the hypothesis of an inhomogeneous poisson process. On the other extreme, if a large number of cells are pooled together, the pooled spike pattern does not satisfy the hypothesis that only one spike has to occur in a sufficiently small, but finite, interval of time. These failures are evident by testing the pooled process to verify if they are indeed poisson. It was found that a good balance is to choose about ten cells for each subpatch. We remark that the subpatches that yield a Poisson process, after pooling, are not the subpatches illustrated in Fig. 4b. Their sizes are smaller than the ones shown in Fig. 4b. Once the retinal patch is subdivided into subpatches, each containing about 10 cells, the pooled processes are obtained for each subpatch. For each subpatch, we construct an intensity function λ_θ which depends on the motion direction θ. When we consider all the subpatches together, we obtain a vector of intensity functions for a vector of inhomogeneous Poisson processes. We use fifty simulations of each angle to generate the intensity function λ_θ or the cumulative spike count function Λ_θ.

From an observation of spike times over a time interval, one can estimate the motion direction $\hat{\theta}$, using a maximum likelihood estimate for inhomogeneous Poisson processes (see [18]). This is done as follows: Let subintervals $[0, t_1)$, $[t_1, t_2)$, $\ldots$, $[t_{k-1}, t_k)$, where $t_k = T$, be the partition of an observation interval $[0, T)$. Let $\boldsymbol{n} = (n_1, n_2, \ldots, n_k)$ be the number of spike occurrence in each of these sub intervals. For a specific observation vector $\boldsymbol{n}$, the log-likelihood function can be written from [18] as:

$$\ell(\theta|\boldsymbol{n}) = -\int_0^T \lambda_\theta(\tau)\,\mathrm{d}\tau + \sum_{j=1}^{k} n_j \ln\left(\int_{t_{j-1}}^{t_j} \lambda_\theta(\tau)\,\mathrm{d}\tau\right). \quad (11)$$

Given the observation $\boldsymbol{n}$, the maximum likelihood estimate of θ is to find θ such that $\ell(\theta|\boldsymbol{n})$ is maximized.

B. Estimation of Speed and Motion Direction

In this subsection, we use data from Simulation II to first estimate the speed of the target.

1) Estimation of the Target Speed: The target speed is estimated by computing the intensity functions over subpatches illustrated in Fig. 4b. Half height pulse widths of these intensity functions are computed next. Finally, the pulse width data is used to estimate the required speed.

Estimating intensity function of a pooled process

For this analysis, we assume that the intensity function of the underlying pooled process is $\lambda(t)$, which depends on the speed and the direction of motion. Thus we may write $\lambda(t) = \lambda(t|v, \theta)$, where v is the speed, θ is the angle of motion. We assume that the intensity function can be decomposed as follows:

$$\lambda(t|v, \theta) = \lambda_0 + \tilde{\lambda}(t|v, \theta), \quad (12)$$

where the first term λ_0 is a constant term, which models the spike activities due to background noise in the retina. The second term $\tilde{\lambda}(t|v, \theta)$ is driven by the input stimulus parameterized by speed v and direction θ.

The first challenge of analyzing the retinal signals under this framework is to estimate the intensity function $\lambda(t|v, \theta)$. It is customary to estimate it using binning methods (see [36], [35], [37]). However, we propose to estimate $\Lambda(t|v, \theta)$ for a combination of v and θ. First of all, for each simulation, we obtain the cumulative spike count upto the time point t. The 'cumulative spike count function' is averaged over all repetitions of simulation for the selected v and θ. The 'mean cumulative spike count function' is smoothed using a smoothing spline or a low pass filter. The resulting smooth function is the required function $\Lambda(t|v, \theta)$. When applying the smoothing algorithm, one has to ensure that $\Lambda(t|v, \theta)$ function is an increasing function, since we require $\lambda(t|v, \theta)$ to be non-negative. Furthermore, we estimate the λ_0 term by considering the response of the patch with no input incident on the retina. Once we obtain the estimates of $\lambda(t|v, \theta)$ for a particular v and θ, using the estimate of λ_0, we can calculate $\tilde{\lambda}(t|v, \theta)$ using (12).

Computing the mean and variance of the half height pulse width

The speed estimates can be obtained by observing the half height pulse width (HHPW) of the $\tilde{\lambda}(t|v, \theta)$ function. We define half height pulse width to be the width of the $\tilde{\lambda}(t|v, \theta)$ function at half its maximum value (see Fig. 5a). The half height pulse width is a good measure of pulse width of a pulse-like signal we have for $\tilde{\lambda}(t|v, \theta)$. It is clear that for faster speed (when the light spot crosses the patch in a shorter time) $\tilde{\lambda}(t|v, \theta)$ is narrower than for slower speed (when the light spot takes a longer time to cross the patch)

From Fig. 5b we can see that it is possible to perform a linear regression between the mean $\mu(v)$ and the time the input takes to cross the patch. Similarly, we can perform another linear regression with standard deviation $\sigma(v)$ and the time the input takes to cross the patch. Note that most of the data points fall within the two lines $\mu(v) \pm \sigma(v)$ in Fig. 5b. Furthermore, assuming Gaussian distribution for the variation of half height pulse width for a particular speed, we can write the likelihood function as a function of speed. Therefore, given a response from the model patch, we can estimate the speed of the target. Under the Gaussian hypothesis, the likelihood function (see [17]) is:

$$L(v|r) = \frac{\exp\left(-(r - \mu(v))^2/2\sigma^2(v)\right)}{\sqrt{2\pi\sigma^2(v)}}. \quad (13)$$

Thus, given an observation (i.e. the half height pulse width) r, the task is to find the speed v that will maximize the likelihood function $L(v|r)$.

2) Detection of the Target Motion Direction: The motion direction is detected either using the poisson process models or using principal component analysis.

Rescaling and Detection of Motion Direction using PPMs

Once we have estimated the target speed v, we modify the activity pattern of each cell in the patch by rescaling the time axis to a $(0, 1)$ interval in seconds. Using the vector point process models presented in subsection VI-A2 on the rescaled activities of each cell, target directions are detected. To avoid repetitions, we omit the details.

Rescaling and Detection of Motion Direction using Voting Methods

Here we restrict our analysis to each and every subpatches described in Fig. 4b. First of all, we compute the intensity function $\tilde{\lambda}(t|v, \theta)$ for the subpatch by considering all the cells in the subpatch. The intensity function is computed by repeating what has already been discussed in subsection VI-B1. Next, the intensity functions are rescaled so that the time axis is normalized to $(0, 1)$ in seconds and the amplitude is scaled so that the associated cumulative spike count $\Lambda(t)$, defined in (9) is 0 at the starting point and 1 at the ending point.

Once the intensity functions are rescaled, we can project them on to a lower dimensional (usually 3 dimensions for display purposes) space. The principal component points can be assumed and verified to be realizations of a multivariate normal distribution, using the Lilliefors [33] test or Kolmogorov-Smirnov (KS) test [34]. Using mean $\boldsymbol{\mu}_\theta = \boldsymbol{\mu}(\theta)$ and $\Sigma_\theta = \Sigma(\theta)$ obtained experimentally, we can write the likelihood function (see [17]), given the k-dimensional observation $\boldsymbol{r}$ from the principal component space to be

$$L(\theta|r) = \frac{\exp\left(-(\boldsymbol{r} - \boldsymbol{\mu}_\theta)^\top \Sigma_\theta (\boldsymbol{r} - \boldsymbol{\mu}_\theta)/2\right)}{\sqrt{2^k \pi^k \left|\Sigma_\theta\right|}}. \qquad (14)$$

We find θ such that $\boldsymbol{\mu}_\theta$ and Σ_θ maximize $L(\theta|r)$, and that θ is the maximum likelihood estimate corresponding to the observation r (see [17]).

The maximum likelihood estimate of the target direction θ is computed for each and every subpatches in Fig. 4b. The final estimated target direction is inferred by taking the majority over all the subpatches using the so called *voting method* (see [20], [19], [41]). The method of voting has been successfully used in many classification problems. The fundamental strategy in this method is to perform classification based on any specific method using a set of classifiers and then make the final classification based on what the majority of the classifiers suggest. The only requirement is that all classifiers should have a detection error less than 0.5.

VII. Results

The main result of this paper is to illustrate the extent to which retinal cells are able to detect direction of target motion. The B cells out perform the A cells in terms of its ability to discriminate motion direction. The superior performance of the B cells over A cells is particularly visible when the target speed is uncertain and is estimated from the retinal response data. We now discuss the results in detail.

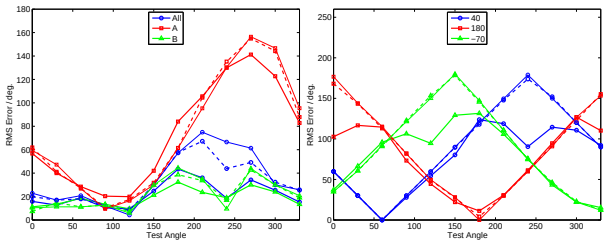

(a) PPM - All cell types (b) PPM - B cells

Fig. 9: For Simulation II, variation of the root mean square error of detection with input angle over different types of cells, using a 100 ms time window starting at 450 ms, in rescaled time. Original *high speed* takes 400 ms (thick solid line), *medium speed* takes 1200 ms (thick dashed line), *low speed* takes 2000 ms (thin line) to cross the patch.

A. Detection of Motion Direction from Simulation I

Recall that in simulation I, the target speed is fixed and known. We restrict cells on the retina to a patch, and apply a double principal component analysis described in subsection VI-A1. The results are shown in Figs. 6a, 6b. From Fig. 6b it can be observed that the direction sensitive 'B cells' detect motion directions with less error close to their preferred directions. If we consider the B cells all together, then the detection error is constant throughout all the motion angles (not displayed in the figure). 'A cells,' on the other hand does not show any variability of detection error with the motion direction.

In Figs. 6c, 6d we plot the root mean square error using the pooled inhomogeneous Poisson process method, described in subsection VI-A2. The displayed results are obtained using a 20 ms window and the window starts at 400 ms, the mid point of the motion of the target in visual space. The Fig. 6c clearly shows the effect of direction sensitive 'B cells.' They out perform the 'A cells' in terms of having a lower root mean square error of detection. Also note that, when all three direction preferences of the 'B cells' are taken together, the overall root mean square error is much lower than any single type and it remains constant over all motion directions.

Fig. 7 show the variation of the root mean square error over time. It can be seen that both PCA and PPM have a better error performance when the target is completely within the retinal patch. Compared to the directional sensitive B cells, the non-directional sensitive A cells have a higher error at 400 ms mark, at which time the stimulus is at the center of the patch.

B. Estimation of Speed and Motion Direction from Simulation II

We present the results of this section in two parts. The first on estimating the speed and the second on detecting the motion direction using rescaled responses.

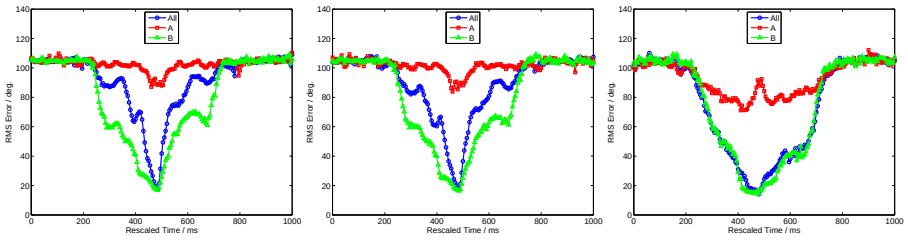

(a) Low Speed (b) Medium Speed (c) High Speed

Fig. 8: For Simulation II variation of the root mean square error of detection over rescaled time using all Cells (blue), A Cells (red) and B Cells (green). Original *high speed* (right) takes 400 ms, *medium speed* (center) takes 1200 ms, *low speed* (left) takes 2000 ms to cross the patch.

1) Estimating Speed: As shown in Fig. 5b, it is possible to establish a linear relation between the time, the spot takes to cross the patch and the half height pulse width. Therefore, we can use the likelihood function (13) to estimate the speed of the moving target. Let T_{EST} be the estimate and T_{ACT} be the actual time to cross the patch with diameter d. Then the speed estimate is d/T_{EST} and the actual speed is d/T_{ACT}. The relative error in speed estimate is described as follows:

$$\text{Relative Error} = \frac{|T_{EST} - T_{ACT}|}{T_{EST}}. \tag{15}$$

We have observed (see [13]) that the root mean square of the relative error as a function of the target speed, is more or less constant. Higher speeds, have a slightly less rms error. Overall, the rms error is about 0.1, i.e. 10% indicating that, it is possible to estimate the speed with a reasonable accuracy.

2) Estimating the Direction of Motion: First step in estimating the direction of motion is to use the estimated speed to rescale the observed activity patterns of the retinal cells. Since the retinal cells are subjected to target inputs at different speeds, the rescaling process normalizes the activity patterns for subsequent detection of motion direction. The target motion directions are now detected using the procedure outlined in subsection VI-B2.

Using the procedure outlined in subsection VI-B2, we illustrate in Figs. 8, 9 the results of detecting direction of motion. The rms error of detection has been plotted in the y-axis. In Fig. 8, we have in the x-axis, the rescaled time indicating detectability of the patch as a function of time. The plots have been repeated at different speeds and for ALL cells, all 'A cells' and all 'B cells.' The plots in this Fig. 8 clearly indicates that for 'B cells,' the detectability increases considerably when the target is around the center of the patch. 'A cells,' on the other hand are unable to detect the target motion direction. We note that this observation is in sharp contrast to what was observed in Fig. 7c wherein the 'A cells' did participate in the detection process although not as strongly as the 'B cells.'

The same detection process is repeated in Fig. 9, where in the x-axis we have all the different angles considered in simulation II. The plots are repeated for different speeds and cell types. The plots in Fig. 9 illustrate that the 'B cells' have an improved ability to detect target direction. Detectability of the 'B cells' changes as a function of the target angle, an expected result. Finally, the discriminability of the 'B cells' in any direction is always better than rms value of approximately 35.

Our final result is on the problem of detecting the target motion direction from the rescaled intensity data using the voting method outlined in subsection VI-B2. We begin by calculating the error probabilities using maximum likelihood detection described in (14) over the different sub-patches. It turns out that the classification error in each sub-patches are less than 0.5. The target motion directions are finally assessed using 'voting method.' When this method is applied, the probability of error is negligible. Hence no result graphs are shown in this paper. Over the pool of test angles used, the voting method was able to classify the correct angle estimate 539 times out of the 540 trials considered.

VIII. Conclusion

Using root mean square of the detection error as a criterion for measuring detectability, we show in this paper that – for the purpose of discriminating motion directions of targets, the motion sensitive 'B cells' are superior compared to the intensity sensitive 'A cells.' The difference in their performance is pronounced particularly when the speed of the target is uncertain and needs to be estimated from the data. We also show that 'B cells' in a retinal patch, located at the center of the turtle's visual streak, with preferred directions set at 40°, 180° and -70° are able to detect, as a population, all angles for target motion direction with the same level of root mean square error.

In this paper, we introduce a new class of algorithms to analyze neuron population, viz. pooling subpatches of neurons and viewing the intensity function of the ensemble as intensity of an inhomogeneous poisson process. Maximum likelihood estimation technique associated with a poisson process discriminates the motion directions of the target.

Although distribution of the A and B cells have been globally computed throughout the entire retina, the analysis presented in this paper is restricted to a patch on the retina. Motion analysis of visual targets throughout the entire retina would be a topic of our future research.

References

[1] Z. Nenadic, B. K. Ghosh, and P. S. Ulinski, "Modeling and estimation problems in the turtle visual cortex," *IEEE Transactions in Biomedical Engineering*, vol. 49, no. 8, pp. 753–762, August 2002.

[2] ——, "Propagating waves in visual cortex: A large scale model of the visual cortex," *Journal of Computational Neuroscience*, vol. 14, pp. 161–184, 2003.
[3] X. Du, B. K. Ghosh, and P. S. Ulinski, "Encoding and decoding target locations with waves in the turtle visual cortex," *IEEE Transactions in Biomedical Engineering*, vol. 52, no. 4, pp. 566–577, April 2005.
[4] ——, "Encoding of motion targets by waves in the turtle visual cortex," *IEEE Transactions in Biomedical Engineering*, vol. 53, no. 8, pp. 1688–1695, August 2006.
[5] W. Wang, C. Campaigne, B. K. Ghosh, and P. S. Ulinski, "Two cortical circuits control propagating waves in visual cortex," *Journal of Computational Neuroscience*, vol. 19, pp. 263–289, 2005.
[6] P. L. Marchiafava and R. Weiler, "Intracellular analysis and structural correlates of the organization of inputs to ganglion cells in the retina of the turtle," *Proceedings of the Royal Society of London. Series B, Biological Sciences*, vol. 208, no. 1170, pp. 103–113, June 1980.
[7] J. Ammermuller, J. F. Muller, and H. Kolb, "The organization of the turtle inner retina. ii. analysis of color-coded and directionally selective cells." *Journal of Comparative Neurology*, vol. 358, no. 1, pp. 35–62, July 1995.
[8] D. B. Bowling, "Light responses of ganglion cells in the retina of the turtle," *Journal of Physiology*, vol. 299, pp. 173–196, February 1980.
[9] E. H. Peterson and P. S. Ulinski, "Qunatitative studies of retinal ganglion cells in a turtle, pseudemys scripta elegans I: Number and distribution of ganglion cells," *Journal of Comparative Neurology*, vol. 186, pp. 17–42, 1979.
[10] ——, "Qunatitative studies of retinal ganglion cells in a turtle, pseudemys scripta elegans II: Size spectrum of ganglion cells and its regional variation," *Journal of Comparative Neurology*, vol. 208, pp. 157–168, 1982.
[11] R. D. Rodieck, *The First Steps in Seeing*. Sinauer, 1998.
[12] A. L. Hodgkin and A. F. Huxley, "A quantitative description of membrane current and its application to conduction and excitation in nerve," *Journal of Physiology*, vol. 117, pp. 500–544, 1952.
[13] M. P. B. Ekanayake, "Decoding the speed and motion direction of moving targets using a turtle retinal patch model," Ph.D. dissertation, Department of Mathematics and Statistics, Texas Tech University, Lubbock, TX 79409, USA., July 2011.
[14] J. Teeters, A. Jacobs, and F. Werblin, "How neural interactions form neural responses in the salamander retina," *Journal of Computational Neuroscience*, vol. 4, no. 1, pp. 5–27, 1997.
[15] F. Worgotter and C. Koch, "A detailed model of the primary visual pathway in the cat: comparison of afferent excitatory and intracortical inhibitory connection schemes for orientation selectivity," *Journal of Neuroscience*, vol. 11, pp. 1959–1979, 1991.
[16] I. T. Jolliffe, *Principal Component Analysis*, 2nd ed., ser. Springer Series in Statistics. Springer, 2002.
[17] H. L. Van Trees, *Detection, Estimation and Modulation Theory, Part I*. John Wiley & Sons Inc., 1968.
[18] D. Snyder, *Random Point Processes*. John Wiley & Sons Inc., November 1975.
[19] S. Theodoridis and K. Koutroumbas, *Pattern Recognition*, 4th ed. Academic Press, 2008.
[20] L. Lam and C. Y. Suen, "Application of majority voting to pattern recognition: An analysis of its behavior and performance," *IEEE Transactions on Systems, Man and Cybernetics - Part A*, vol. 27, no. 5, pp. 553–568, 1997.
[21] J. R. Dearworth and A. M. Granda, "Multiplied functions unify shapes of ganglion-cell receptive fields in retina of turtle," *Journal of Vision*, vol. 2, no. 3, pp. 204–217, 2002.
[22] E. M. Lasater and P. Witkovsky, "Membrane currents of spiking cells isolated from turtle retina," *Journal of Comparative Physiology A.*, vol. 167, no. 1, pp. 11–21, 1990.
[23] Y. Liu and E. M. Lasater, "Calcium currents in turtle retinal ganglion cells. i. the properties of t- and l-type currents," *Journal of Neurophysiology*, vol. 71, no. 2, pp. 733–742, 1994.
[24] T. I. Baker and P. S. Ulinski, "Models of direction selective and non-direction selective turtle retinal ganglion cells," *Society for Neuroscience Abstract*, 2001.
[25] D. A. Baylor and A. L. Hodgkin, "Detection and resolution of visual stimuli by turtle photoreceptors," *Journal of Physiology*, vol. 234, pp. 163–198, 1973.
[26] A. M. Granda and J. E. Fulbrook, "Classification of the turtle ganglion cells," *Journal of Neurophysiology*, vol. 62, pp. 723–737, 1989.
[27] D. Tranchina, J. Gordon, and R. M. Shapely, "Retinal light adaptation evidence for feedback mechanism," *Nature*, vol. 310, pp. 314–316, 1984.
[28] L. J. Borg-Graham, "The computation of directional selectivity in the retina occurs presynaptic to the ganglion cell," *Nature Neuroscience*, vol. 4, pp. 176–183, 2001.
[29] S. Iyengar and Q. Liao, "Modeling neural activity using the generalized inverse gaussian distribution," *Biological Cybernetics*, vol. 77, pp. 289–295, 1997.
[30] MathWorks, "Matlab," 2009. [Online]. Available: http://www.mathworks.com/products/matlab/
[31] J. M. Bower and D. Beeman, *The Book of GENESIS: Exploring Realistic Neural Models with GEneral NEural SImulation System*, 2nd ed. Springer Telos, 1998.
[32] D. L. Snyder and M. I. Miller, *Random Point Processes in Time and Space*, ser. Springer Texts in Electrical engineering, J. B. Thomas, Ed. Springer-Verlag, 1991.
[33] H. Lilliefors, "On the kolmogorov–smirnov test for normality with mean and variance unknown," *Journal of the American Statistical Association*, vol. 62, pp. 399–402, June 1967.
[34] F. J. Massey, "The Kolmogorov-Smirnov test for goodness of fit," *Journal of the American Statistical Association*, vol. 46, no. 253, pp. 68–78, 1951.
[35] U. T. Eden, L. M. Frank, R. C. Barbieri, V. Solo, and E. N. Brown, "Dynamic analysis of neural encoding by point process adaptive filtering," *Neural Computation*, vol. 16, no. 5, May 2004.
[36] E. N. Brown, R. C. Barbieri, V. Ventura, R. E. Kass, and L. M. Frank, "The time-rescaling theorem and its applications to neural spike train data analysis," *Neural Computation*, vol. 14, pp. 325–346, 2001.
[37] A. R. C. Paiva, "Reproducing kernel hilbert spaces for point processes, with applications to neural activity analysis," Ph.D. dissertation, University of Florida, 2008.
[38] M. B. Egerstedt and C. F. Martin, *Control Theoretic Splines: Optimal Control, Statistics and Path Planning*, ser. Princeton Series in Applied Mathematics. Princeton University Press, 2010.
[39] G. Wahba, *Spline models for Observational Data*, ser. CBMS-NSF Regional Conference Series in Applied Mathematics. SIAM, 1990.
[40] G. Casella and R. L. Berger, *Statistical Inference*, 2nd ed. Duxbury Press, June 2001.
[41] D. J. Miller and L. Yan, "Critic-driven ensemble classification," *IEEE Transactions on Signal Processing*, vol. 47, no. 10, pp. 2833–2844, 1999.

Mervyn P. B. Ekanayake received the B.Sc. degree in electrical and electronic engineering from the University of Peradeniya, Sri Lanka, in 2006, and Ph.D. degree in mathematics from the Texas Tech University in 2011. His research interest includes modeling biological systems and biomedical signal processing.

Bijoy K. Ghosh (S'78 – M'79 – SM'90 – F'00) received the B. Tech. and M. Tech. degrees in Electrical and Electronics Engineering from BITS, Pilani, and the Indian Institute of Technology, Kanpur, India, and the Ph.D. degree in Applied Mathematics from the Decision and Control Group of the Division of Applied Sciences, Harvard University, Cambridge, MA, in 1977, 1979, and 1983, respectively. From 1983 to 2006, he has been a faculty member in the Department of Electrical and Systems Engineering, Washington University, St. Louis, MO, as a professor, and directed the center for BioCybernetics and Intelligent Systems. Presently he is a Dick and Martha Brooks Endowed Professor in the Department of Mathematics and Statistics at Texas Tech University, Lubbock, TX.

Philip S. Ulinski received the Ph.D. degree in zoology from Michigan State University, East Lansing, in 1968. He was Professor and Chairman of the Committee on Computational Neuroscience at the University of Chicago, Chicago, IL. His research interests had been the functional organization of the cerebral cortex and computational models of neural circuits.